Ore Geology Reviews 69 (2015) 403–416

Contents lists available at ScienceDirect

Ore Geology Reviews

journal homepage: www.elsevier.com/locate/oregeorev

Age and petrogenesis of Anisian magnesian alkali basalts and their genetic association with the Kafang stratiform Cu deposit in the Gejiu supergiant tin-polymetallic district, SW China

Jiawei Zhang [a,b], Chuangu Dai [a], Zhilong Huang [b,*], Taiyi Luo [b], Zhikuan Qian [c], Ying Zhang [d]

[a] Guizhou Geological Survey, Bureau of Geology and Mineral Exploration and Development of Guizhou Province, Guiyang 550005, China
[b] State Key Laboratory of Ore Deposit Geochemistry, Institute of Geochemistry, Chinese Academy of Sciences, Guiyang 550081, China
[c] Architectural Engineering College, Guizhou Mingzu University, Guiyang 550025, China
[d] Department of Resource and Environmental Engineering, Guizhou Institute of Technology, Guiyang, 550003, China

ARTICLE INFO

Article history:
Received 30 October 2014
Received in revised form 13 March 2015
Accepted 16 March 2015
Available online 19 March 2015

Keywords:
Gejiu basalts
Kafang stratiform Cu deposit
Ore genesis
Tectonic setting
Hydrothermal alteration
SW China

ABSTRACT

Gejiu is geographically located near Gejiu city, SW China. It is one of the largest tin-polymetallic districts in the world and contains approximately 3 million tons (Mt) of Sn and smaller quantities of Cu, Pb, and Zn. The deposit primarily yields three different types of ore: skarn-hosted ore, basalt-hosted stratiform ore, and carbonate-hosted stratiform ore. Kafang is one of the primary ore deposits in the Gejiu district and is an unusual occurrence hosted in basaltic rocks. Genetic models of the Kafang deposit suggest that it is related either to Anisian (Lower stage of Middle Triassic) Gejiu basalts or to Cretaceous Gejiu granite. In this study, we performed zircon SIMS U–Pb dating, major and trace element analyses, and Sr–Nd–Pb isotopic analyses for the Gejiu basalts and S isotopic analyses for stratiform Cu ore. Our results and previous studies are used to interpret the petrogenesis of the Gejiu basalts and the origin of the basalt-hosted stratiform Cu deposit. The SIMS zircon U–Pb analyses of the Gejiu basalts yield an age of 244.4 Ma. The trace element ratios of the Gejiu basalts are similar to those of ocean island basalt and have positive $\varepsilon Nd(t)$ values (ranging from 0.6 to 2.5) and uniform $(^{87}Sr/^{86}Sr)_i$ values (ranging from 0.70424 to 0.70488). These ratios are close to those of the Permian Emeishan flood basalt. Thus, the Gejiu basalts may represent coeval volcanisms within the plate involving remelting of the Emeishan plume head through a stress relaxation process after the main plume event. The Pb and S isotopic compositions of the Gejiu basalts and the stratiform Cu ores indicate that the source of Cu and S is primarily derived from the Gejiu basalts. However, the age of sulfide mineralization (84.2–79.6 Ma) and the age of hydrothermal alteration (85.5–81.9 Ma) are temporally consistent with the age of the Cretaceous granite emplacement (85.5–83.3 Ma). From a petrological and geochemical study, we determine that the Gejiu basalts may have been subjected to pervasive granite-related hydrothermal alteration during the emplacement of granite. These processes increase the K and Mg contents of basalt and probably caused the formation of the Cu ores. Thus, the Kafang stratiform Cu deposit can be considered as a granite-related hydrothermal deposit.

1. Introduction

The southern part of China is composed of two major blocks, the Yangtze and the Cathaysia blocks. The ocean between the Yangtze and the Cathaysia blocks closed at approximately 1000 to 900 Ma (e.g., Li et al., 2007). The Gejiu district is tectonically located to the west end of the Cathaysia block and is bounded by the Yangtze block to the north and the Red River fault to the south. This district is also located in the southern part of the intermediate zone (Xu et al., 2004) of the Permian Emeishan Large Igneous Province (ELIP) (Fig. 1a). Gejiu is one of the largest tin districts in the world. It contains approximately 3 million tons (Mt) of Sn and smaller amounts of Cu, Pb, and Zn. Several parallel EW-trending faults and two NE-trending faults in the eastern part control the general configuration of the mineralization and distribution of five polymetallic deposits in the Gejiu district from north to south (Fig. 1c): the Malage, Songshujiao, Gaosong, Laochang, and Kafang deposits. Three types of ore are primarily found in the Gejiu district: (1) skarn-hosted ore, (2) Anisian basalt-hosted stratiform ore, and (3) Middle Triassic Gejiu Formation carbonate-hosted stratiform ore. The origin of the Gejiu deposits and the mechanism for such an accumulation of Sn–Cu–Pb–Zn have long been controversial. Most researchers believe the skarn-type ore to be genetically related to Late Cretaceous granite (e.g., 308 Geological Party, 1984; Zhuang et al., 1996; Mao et al., 2008; Cheng et al., 2013). Recently, the age of the granite has been constrained to 85.5–83.3 Ma (Cheng and Mao, 2010); the age of mineralization (95.3 to 77.4 Ma) is also confirmed by the ^{40}Ar–^{39}Ar dating of muscovite and phlogopite and by the Re–Os dating

* Corresponding author.
E-mail address: huangzhilong@vip.gyig.ac.cn (Z. Huang).

http://dx.doi.org/10.1016/j.oregeorev.2015.03.011
0169-1368/

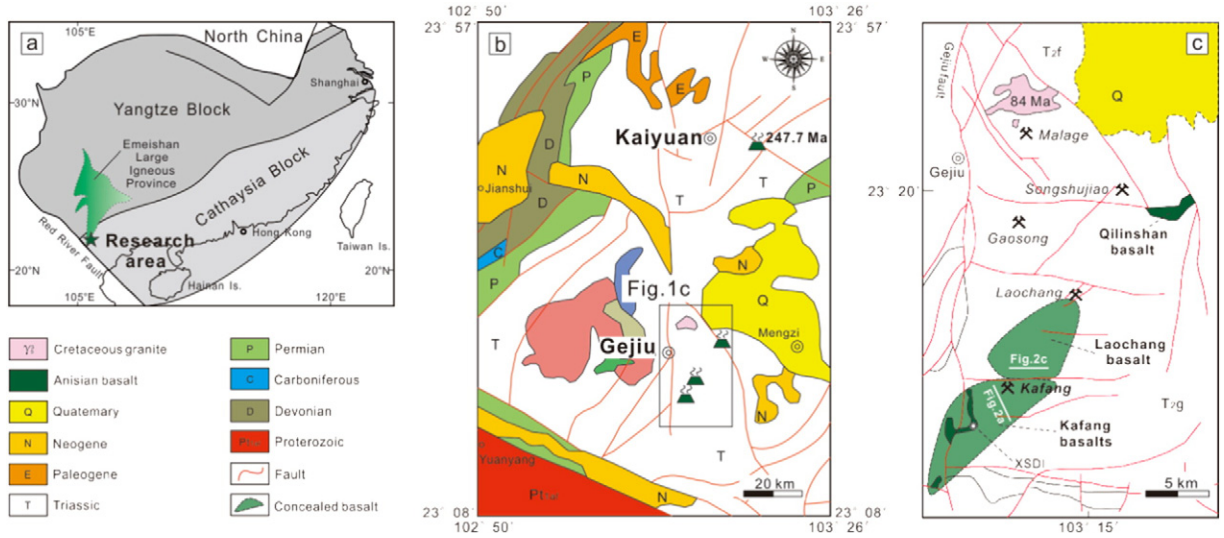

Fig. 1. (a) Simplified tectonic map showing the study area in relation to South China's major tectonic units and the Emeishan Large Igneous Province district (Li et al., 2007; Xu et al., 2004). (b) Geological map of the Gejiu–Kaiyuan district. (c) Geological map of the Gejiu district. The green regions with dashed borders are the vertical projections of underground basalts.

of molybdenite (Cheng et al., 2012, 2013). However, because many ore bodies are approximately stratiform, the origin of the basalt-hosted and carbonate-hosted stratiform ore has been proposed as syngenetic, belonging to the volcanogenic massive sulfide (VMS) and the sedimentary-exhalative (SEDEX) deposits, respectively (e.g., Li, 1991; Tan et al., 2006; Li et al., 2006; Zhang et al., 2007; Lu, 2008; Qian, 2012).

Although the amount of research regarding granite-related hydrothermal origins has been growing substantially, the Gejiu basalts remain an important key to resolving these debates from another aspect because the geochemistry of the basalts is critical to revealing the petrogenesis and the relationship between the volcanism and the associated stratiform ore. Previous studies imply that the Gejiu basalts were once viewed as a set of mafic–ultramafic rock assemblages with high K and Mg contents that were deposited on the extensional continental plate (e.g., Li et al., 2008; Y.S. Li et al., 2009; Zhang et al., 2009; Fang and Jia, 2011). A contemporary Anisian-age magmatism has also been discovered in the Kaiyuan district. Zhang et al. (2013, 2014) suggested that the Gejiu and Kaiyuan basalts are the remelting products of the Emeishan plume at 247.7 Ma after the main Emeishan plume event (260–257 Ma, from Shellnutt et al., 2012). However, these studies fail to explain the association between the basalts and the Kafang stratiform Cu deposit. Although detailed petrological and geochemical studies have been undertaken on the Gejiu basalts, several questions remain unresolved: (1) The precise eruption age of the Gejiu basalts is uncertain. (2) The source of ore-forming material of the stratiform Cu deposit needs to be confirmed by additional evidence such as Pb and S isotopic compositions of both basalt and ore. (3) The geochemistry of the Gejiu basalts is largely different from that of the Kaiyuan basalt. How the Gejiu basalts with high K and Mg contents were generated and whether these characteristics are related to the ore-forming process need to be explained. (4) Due to the lack of the eruption age and Sr–Nd isotopic data, the tectonic setting and the mantle source of the basalt remain unclear. These four problems are critical to resolve whether the basalt-hosted stratiform Cu deposit is a VMS deposit.

This study builds on previous research, and incorporates field investigation, zircon SIMS U–Pb data, major and trace element composition, Sr–Nd–Pb isotopic composition of the Gejiu basalts, and the S isotopic composition of the Kafang stratiform Cu deposit, with the aims of (1) constraining the timing of the Gejiu basalts, (2) investigating the origin of the Kafang stratiform Cu deposit, and (3) determining the cause of the abnormal K and Mg to reveal the tectonic and mantle source of the Gejiu basalts. Finally, the results are integrated into a genetic model of the Kafang stratiform Cu deposit.

2. Geological setting

The Gejiu district underwent a long, complex history of tectonic activity, which led to a series of faulting and folding structures at various scales (Cheng and Mao, 2010). The NS-trending Gejiu fault divides the Gejiu district into eastern and western parts. The Kafang deposit is located in the southernmost part of the Gejiu district. Different from other deposits in the Gejiu district, which are characterized by dominant Sn mineralization, the Kafang deposit contains only Cu, with defined reserves of approximately 0.4 Mt of Cu. The ores consist of several layers (stratiform) hosted in the Gejiu basalt.

Lithologies in the district are made up of a 3-km-thick sequence of Permian and Triassic clastic rocks with interlayered basaltic lavas in the Middle Triassic sequence. The rocks comprise of ~400–1400 m of Gejiu Formation carbonates with intercalations of Anisian (Lower stage of Middle Triassic) basaltic lavas. These carbonates and the interlayered basaltic lavas are the most important ore-hosting strata. According to Xue (2002) and YBGMR (1982), these lavas are in both Gejiu and Kaiyuan districts (Fig. 1b). Recently, the age of Kaiyuan basalts (247.7 ± 1.7 Ma) has been constrained by Zhang et al. (2014).

Cretaceous igneous rocks are emplaced in both the eastern and the western parts of Gejiu district. The granite primarily intrudes the eastern part of the Gejiu Formation, with ages of 85.5–83.3 Ma (Fig. 2). The granite has two types of texture: porphyritic and equigranular. Both originate from the same granite magma that experienced different degrees of fractional crystallization. The equigranular granite is mostly distributed deep underground and only sporadically in the south Laochang and Kafang areas (Cheng and Mao, 2010).

3. Field geology and petrography

3.1. The Gejiu basalts

The Gejiu basalts cover an area of >125 km^2. The basalt is mostly unexposed and hosted in the lower part of the Gejiu Formation. The basalt samples were collected at three different sites, the Kafang (KF), the Laochang (LC), and the Qilinshan (QLS) (Fig. 1c). The details of the samples are listed in Table 1.

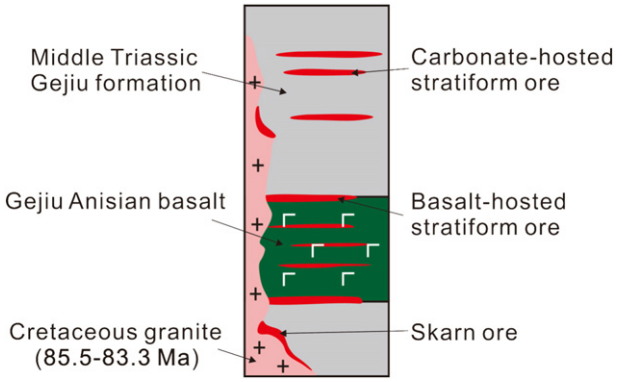

Fig. 2. Stratigraphic column of the Gejiu deposit.

The KF and LC basalts are conformably interbedded with sedimentary units of the Gejiu Formation (Fig. 3a and c). The basalts dip to the northwest at an angle of 10°–30°. The thickness of a single layer of the basalt ranges from 0.05 to 30 m, and the total thickness is >100 m (Wang, 1993). There are several marble lenses interbedded with the basalt. Whole-rock samples were collected from the Qianjin adit in the Kafang deposit (1800 m above sea level) and from the #130 adit in the LC deposit (1710 m above sea level). The samples were collected along strike at ≈50-m intervals. The KF and LC basalts could barely be distinguished by their petrological characteristics alone. The basalts are primarily dark green or dark gray in color, and exhibit massive and amygdaloidal structures. The schistosity is extensively developed, and the primary textures are intergranular and intersertal. The primary fabrics and mineralogy of the fresh basalt are uncertain because the KF and LC basalts are overprinted by pervasive late-stage alteration. The alteration minerals are phlogopite, actinolite, chlorite, tremolite and biotite. The accessory minerals include ilmenite, magnetite and sulfides (Fig. 4a). Sulfide mineralization is hosted by the KF and LC basalts (Fig. 4b). Significantly, some of the KF basalts that are spatially close to the granite have undergone intense alteration and have been largely transformed into diopsidite. Qian (2012) reported the geological and geochemical characteristics of this rock type, and suggested that a hydrothermal activity occurred simultaneously with the basalt eruption.

The outcrop of the QLS basalt is situated in the eastern part of the Songshujiao deposit. The exposed QLS basalt has been referred to as part of the KF and LC basalts by previous studies (e.g., Li et al., 2006). A large volume of the QLS basalt is pervasively weathered (Fig. 3e). Our sampling location at N 23°19′16.4″, E 103°17′3.8″, 1771 m above sea level, is an underground adit, which made it feasible to obtain unaltered samples of the QLS basalt. These samples were collected along strike at ≈20-m intervals. The QLS basalt is dark green, with amygdales. The amygdales are asymmetrical, being 0.2–2 cm in diameter and having a preferred orientation. The amygdales are primarily filled with chalcedony with manifold sharp edges and asymmetrical texture. Unlike the KF and LC basalts, the minerals of the QLS basalt underwent little alteration or mineralization. The basalt is primarily composed of oriented plagioclase, and fine-grained clinopyroxene, ilmenite and magnetite (Fig. 4c and d).

3.2. The Kafang stratiform Cu deposit

The stratiform Cu ores are hosted in the KF basalt in the Qianjin adit, 1800 m above sea level. Generally, the sheet-like basalt-hosted ores are about ~200–400 m in length, and the thickness ranges between 0.1 and 10 m. The Cu contents of the stratiform ores are generally higher toward the hosted basalt and are commonly lower toward the wall rock. The contacts between ore and basalt and between ore and wall rock are clear, as shown in Fig. 5a. The ore minerals are dominated by chalcopyrite and pyrrhotite, and these two minerals in hand specimens exhibit an alternating layer structure (Fig. 5b) and idiomorphic or hypidiomorphic granular texture under a microscope. The gangue minerals include phlogopite, actinolite, calcite, tremolite, and chlorite. Phlogopite and actinolite are intergrown with chalcopyrite and pyrrhotite. The basalt underwent phlogopite alteration and sulfide mineralization while the nearby Gejiu Formation experienced marmorization.

Table 1
Details of the samples used in this study.

Sample	Lithology	Location	Altitude	Mineral association
KF-1	Amygdaloidal basalt	Kafang Qianjin adit	1800 m	Phlogopite + plagioclase + clinopyroxene + ilmenite + magnetite
KF-2	Amygdaloidal basalt	Kafang Qianjin adit	1800 m	Phlogopite + plagioclase + clinopyroxene + ilmenite + magnetite + sulfides
KF-3	Amygdaloidal basalt	Kafang Qianjin adit	1800 m	Phlogopite + actinolite + clinopyroxene + ilmenite
KF-4	Massive basalt	Kafang Qianjin adit	1800 m	Phlogopite + plagioclase + clinopyroxene + ilmenite + magnetite
KF-5	Massive basalt	Kafang Qianjin adit	1800 m	*Phlogopite + tremolite + chlorite + ilmenite + magnetite + sulfides*
KF-6	Massive basalt	Kafang Qianjin adit	1800 m	Phlogopite + actinolite + chlorite + ilmenite + magnetite
KF-7	Massive basalt	Kafang Qianjin adit	1800 m	Phlogopite + actinolite + tremolite + chlorite + ilmenite + magnetite + sulfides
KF-8	Massive basalt	Kafang Qianjin adit	1800 m	Phlogopite + actinolite + ilmenite + magnetite + sulfides
KF-9	Massive basalt	Kafang Qianjin adit	1800 m	Phlogopite + tremolite + chlorite + ilmenite + magnetite + sulfides
LC-1	Massive basalt	Laochang Zhuyeshan #130 adit	1710 m	Phlogopite + actinolite + plagioclase + ilmenite + magnetite
LC-2	Amygdaloidal basalt	Laochang Zhuyeshan #130 adit	1710 m	Biotite + actinolite + plagioclase + ilmenite + magnetite
LC-3	Massive basalt	Laochang Zhuyeshan #130 adit	1710 m	Phlogopite + actinolite + plagioclase + clinopyroxene + ilmenite
LC-4	Amygdaloidal basalt	Laochang Zhuyeshan #130 adit	1710 m	Phlogopite + actinolite + plagioclase + ilmenite + magnetite + sulfides
LC-5	Massive basalt	Laochang Zhuyeshan #130 adit	1710 m	Phlogopite + actinolite + plagioclase + ilmenite + magnetite
LC-6	Massive basalt	Laochang Zhuyeshan #130 adit	1710 m	Phlogopite + actinolite + tremolite + ilmenite + magnetite + sulfides
LC-7	Massive basalt	Laochang Zhuyeshan #130 adit	1710 m	Tremolite + biotite + chlorite + ilmenite + magnetite + sulfides
LC-8	Massive basalt	Laochang Zhuyeshan #130 adit	1710 m	Tremolite + biotite + chlorite + ilmenite + magnetite + sulfides
LC-9	Massive basalt	Laochang Zhuyeshan #130 adit	1710 m	Phlogopite + actinolite + plagioclase + clinopyroxene + ilmenite
QLS-1	Amygdaloidal basalt	N 23°19′16.4″, E 103°17′3.8″	1771 m	Plagioclase + clinopyroxene + ilmenite + magnetite
QLS-2	Amygdaloidal basalt	N 23°19′16.4″, E 103°17′3.8″	1771 m	Plagioclase + clinopyroxene + ilmenite + magnetite
QLS-3	Amygdaloidal basalt	N 23°19′16.4″, E 103°17′3.8″	1771 m	Plagioclase + clinopyroxene + ilmenite + magnetite
QLS-4	Amygdaloidal basalt	N 23°19′16.4″, E 103°17′3.8″	1771 m	Plagioclase + clinopyroxene + ilmenite
QLS-5	Amygdaloidal basalt	N 23°19′16.4″, E 103°17′3.8″	1771 m	Plagioclase + clinopyroxene + ilmenite + magnetite
QLS-6	Amygdaloidal basalt	N 23°19′16.4″, E 103°17′3.8″	1771 m	Plagioclase + clinopyroxene + ilmenite + magnetite
QLS-7	Amygdaloidal basalt	N 23°19′16.4″, E 103°17′3.8″	1771 m	Plagioclase + clinopyroxene + ilmenite + magnetite
QLS-8	Amygdaloidal basalt	N 23°19′16.4″, E 103°17′3.8″	1771 m	Plagioclase + olivine + clinopyroxene + ilmenite + magnetite
QLS-9	Amygdaloidal basalt	N 23°19′16.4″, E 103°17′3.8″	1771 m	Plagioclase + olivine + clinopyroxene + ilmenite + magnetite
QLS-10	Amygdaloidal basalt	N 23°19′16.4″, E 103°17′3.8″	1771 m	Plagioclase + clinopyroxene + ilmenite + magnetite
QLS-11	Amygdaloidal basalt	N 23°19′16.4″, E 103°17′3.8″	1771 m	Plagioclase + clinopyroxene + ilmenite + magnetite

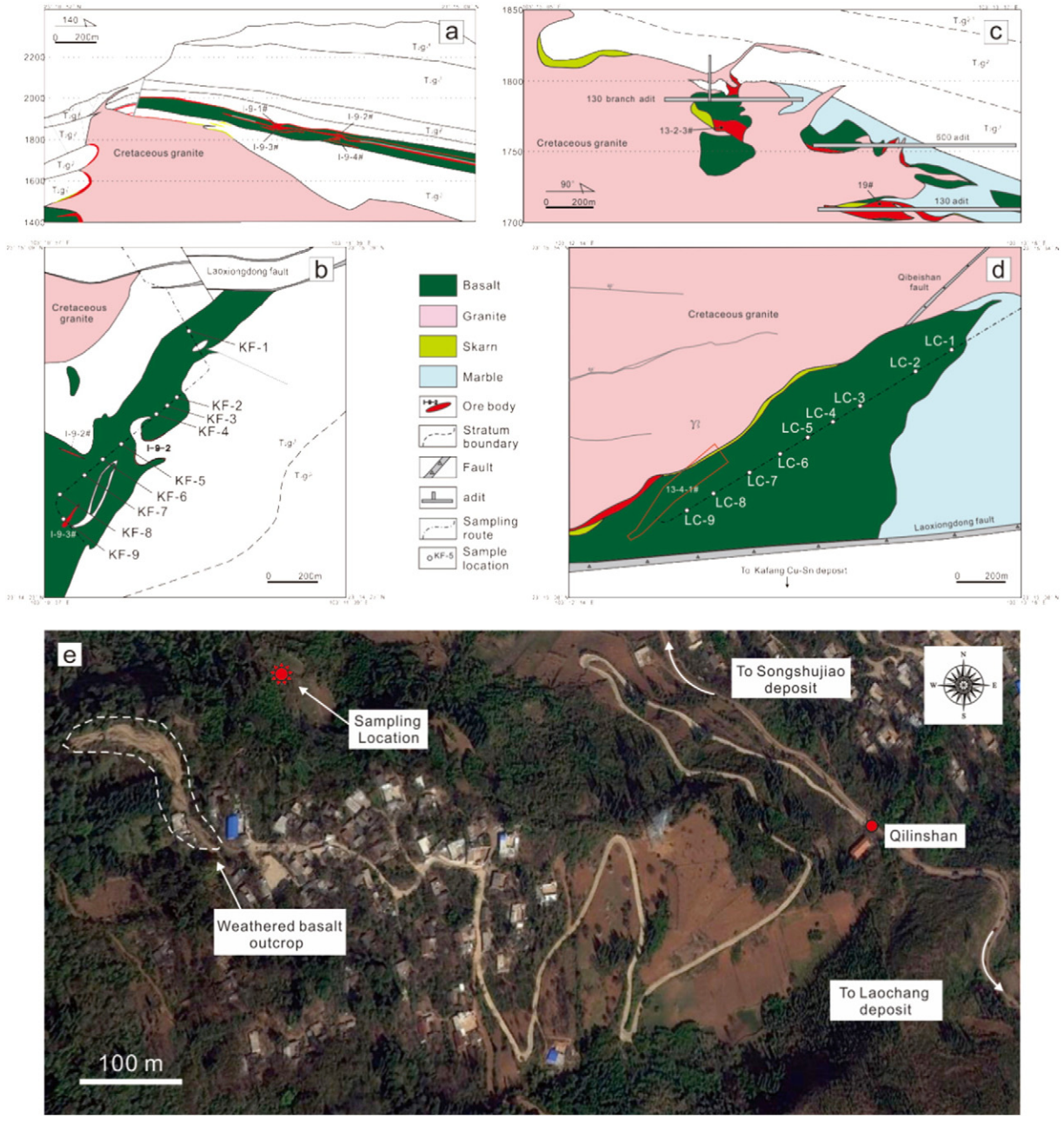

Fig. 3. (a) Geologic section of basalts in the Kafang deposit. (b) Detailed map of basalts in the Kafang deposit (height = 1800 m) and sampling locations. (c) Geologic section of basalts in the LC deposit. (d) Detailed map of basalts in the LC deposit (height = 1710 m) and sampling locations. (e) Sampling locations of the QLS basalts.

4. Analytical procedures

4.1. Zircon SIMS U–Pb dating

The altered basalt sample XSDI from south Kafang district was selected for the chronological study. For cathodoluminescent (CL) imaging, representative zircon grains were handpicked, mounted in epoxy resin disks, subsequently polished and coated with carbon. The internal morphology was examined using CL prior to U–Pb isotopic analyses. Zircon U–Pb dating was conducted using a Cameca SIMS 1280 ion microprobe (CASIMS) at the Institute of Geology and Geophysics, Chinese Academy of Sciences. During analyses of the zircons, the standard zircon 91500 was used to calibrate the Pb/U ratio and U concentration. The analytical procedures used were similar to those described by X.H. Li et al. (2009). The measured Pb isotopic compositions were corrected for common Pb using non-radiogenic ^{204}Pb. The average uncertainty for measured ratios (except for spot XSDI@5) of ^{206}Pb/^{238}U was 1.6%, and the calculated weighted mean ages are within 95% confidence limits. The age computations and concordia diagrams were made using Isoplot (version 3.0) (Ludwig, 2003).

4.2. Whole-rock major and trace element analyses

Nine KF basalts, nine LC basalts and eleven QLS basalts were selected for whole-rock major element analyses. The analyses were performed by the Mineral-Chemex Division of ALS Laboratory Group (Guangzhou, China). The calcined or ignited sample for major element analyses (0.9 g) was added to 9.0 g of lithium borate flux (50%–50% $Li_2B_4O_7$–$LiBO_2$), mixed well and fused in an auto fluxer at a temperature of 1050–1100 °C. A flat molten glass disk was prepared from the resulting melt. This disk was then analyzed using X-ray fluorescence spectrometry. The uncertainties were ≤2% for the major elements.

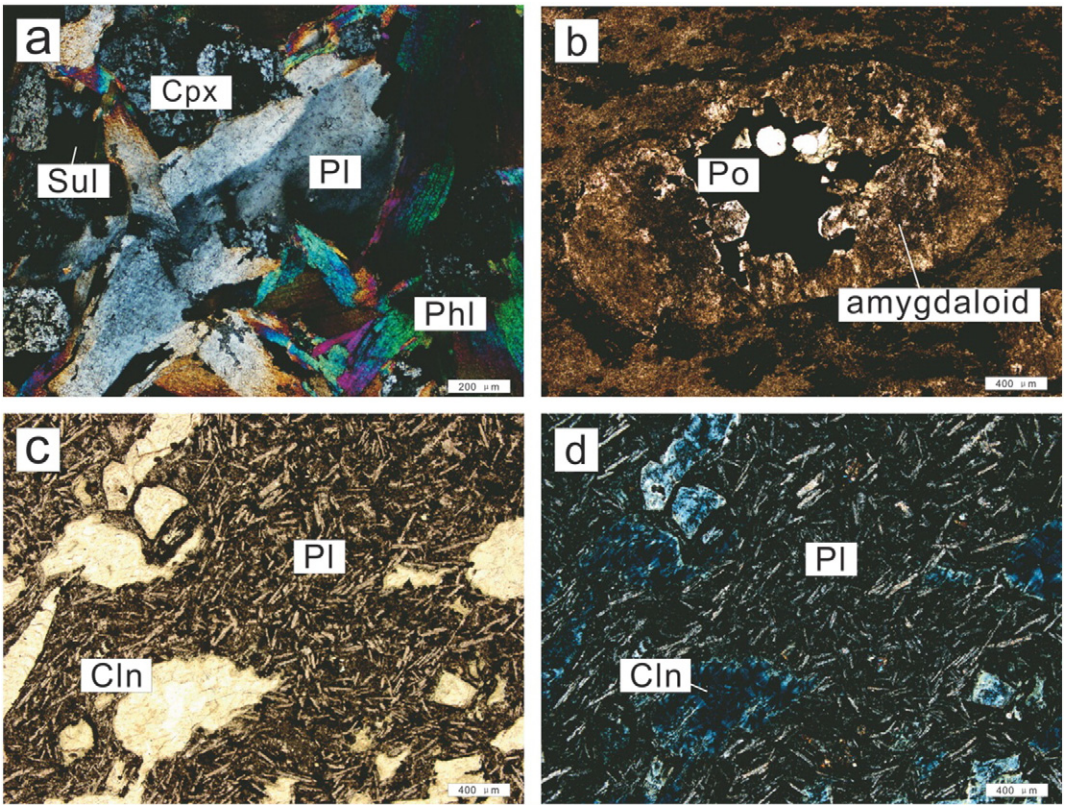

Fig. 4. (a) KF basalt, showing phlogopite (Phl), clinopyroxene (Cpx), plagioclase (Pl), and sulfide (Sul); image is from Zhang et al. (2012a). (b) KF basalt, showing amygdale filled with pyrrhotite (Po). (c) QLS basalt, showing chalcedony (Cln) amygdales and groundmass plagioclase. (d) QLS basalt.

The samples were analyzed for trace elements using a Perkin–Elmer Sciex ELAN DRC-e inductively coupled plasma mass spectrometer (ICP-MS) at the Institute of Geochemistry, Chinese Academy of Sciences after a 36-hour digestion using a mixture of HF and HNO_3 acids in high-pressure bombs following the procedure of Liang et al. (2000). Standard additions, pure elemental standards for external calibration, and GBPG-1, AMH-1, and OU-6 as reference materials were used. The uncertainties were ≤10% for the majority of the trace elements.

4.3. Analyses of Rb–Sr and Sm–Nd isotopic compositions

Six QLS basalts (QLS-6 to QLS-11) were selected for the Rb–Sr and Sm–Nd isotopic measurements using a MAT-262 TIMS at the Institute of Geochemistry, Chinese Academy of Sciences. The chemical separation and isotopic measurement procedures followed Zhang et al. (2002). The sample powders were leached in purified 6 N HCl for 24 h at room temperature to minimize the influence of surface alteration or weathering, especially for Sr isotopic ratios. Sample powders were spiked with mixed isotope tracers, then dissolved in Teflon capsules with HF and HNO_3. Sr and REE fractions were separated in solution using cationic ion-exchange resin columns. Nd was separated from REE fractions using cationic ion-exchange columns and P507 extraction and eluviation resin. The collected Sr and Nd fractions were evaporated and dissolved in 2% HNO_3 to yield solutions for analysis by mass spectrometry. The mass fractionation corrections for the Sr and Nd isotopic ratios was based on ratios of $^{86}Sr/^{88}Sr = 0.1194$ and $^{146}Nd/^{144}Nd = 0.7219$, respectively. The analyses of the standards during the period of analyses were as follows: the NBS987 Sr standard yielded a $^{87}Sr/^{86}Sr$ ratio of 0.710250 ± 0.000007, and the JNdi-1 Nd standard yielded a $^{143}Nd/^{144}Nd$ ratio of 0.512109 ± 0.000005, which were in agreement with reference values

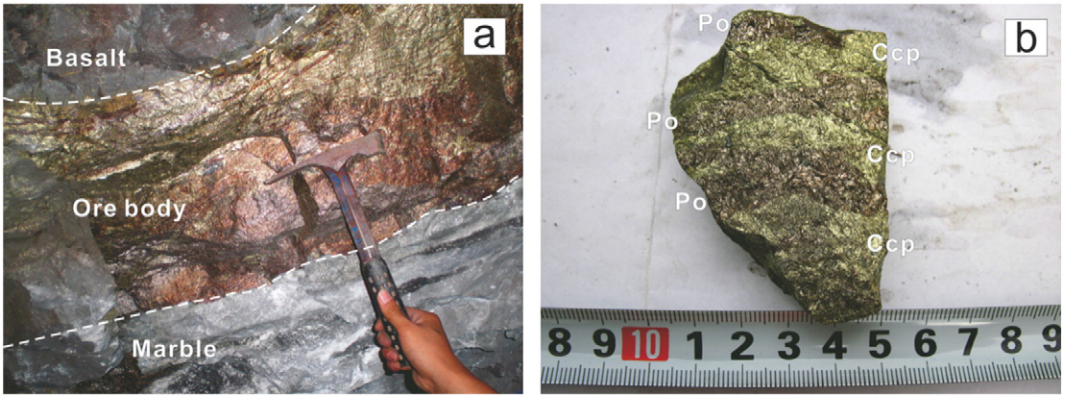

Fig. 5. (a) Outcrop of the Kafang stratiform Cu ore body. (b) Hand specimen of basalt-hosted stratiform ore.

(0.710248 for $^{87}Sr/^{86}Sr$, 0.512115 for $^{143}Nd/^{144}Nd$). The average uncertainties for measured Rb–Sr and Sm–Nd ratios were 0.000005 and 0.000002, respectively.

4.4. Analyses of Pb isotopic compositions

Three KF basalts (KF-5, KF-8 and KF-9) and six QLS basalts (QLS-6 to QLS-11) were selected for the Pb isotope analyses. The analyses were carried out using a GV Isoprobe-T thermal ionization mass spectrometer (TIMS) at the Beijing Institute of Uranium Geology. The analytical procedure involved dissolution of samples using HF and $HClO_4$ in crucibles, followed by basic anion exchange resin to purify Pb (Zhang et al., 2002). Analytical results for the standard NBS981 are $^{208}Pb/^{204}Pb = 36.611 \pm 0.004$ (2σ), $^{207}Pb/^{204}Pb = 15.457 \pm 0.002$ (2σ) and $^{206}Pb/^{204}Pb = 16.937 \pm 0.002$ (2σ), in agreement with the reference value (Belshawet et al., 1998). The average 2σ uncertainties for measured ratios of $^{206}Pb/^{204}Pb$, $^{207}Pb/^{204}Pb$ and $^{208}Pb/^{204}Pb$ were 0.002, 0.002 and 0.005, respectively.

4.5. Analyses of S isotopic compositions

A total of 23 sulfides (chalcopyrite and pyrrhotite) which had been separated from the representative stratiform Cu ore in Kafang Qianjin adit were selected. The samples were weighed (60–70 μg) and combusted in an elemental analyzer furnace at 1030 °C to prepare SO_2 for the S isotope analyses. The analyses were carried out using a continuous flow stable isotope ratio mass spectrometer (CF-IRMS) at the Institute of Geochemistry, Chinese Academy of Sciences. The internal standard used was 04415 Ag_2S. $\delta^{34}S$ values are reported relative to the Canyon Diablo Troilite (CDT). The average standard deviation (SD) for measured ratios was 0.03‰.

5. Results

5.1. Zircon SIMS U–Pb geochronology

The zircon U–Pb analytical results are reported in Table 2. Three types of zircon have been classified based on weighted mean $^{206}Pb/^{238}U$ age, $f^{206}Pb\%$, and Th and U contents: (1) basaltic zircon, (2) hydrothermal zircon, and (3) inherited zircon.

(1) The basaltic zircons are 100–150 μm in size and exhibit euhedral appearance with light and visible magmatic oscillatory zoning. Inclusions, cores, and cracks are absent, as shown in the cathodoluminescence (CL) images (Fig. 6a). The $f^{206}Pb\%$ value is low, ranging from 0.05 to 3.4. These zircons have a relatively wide range in Th (105–1142 ppm) and U (256–1416 ppm) contents, with Th/U ratios ranging from 0.19 to 1.10. All 21 zircon grains fall within a single population with a weighted mean $^{206}Pb/^{238}U$ age of 244.4 ± 2.8 Ma (MSWD = 2.8) (Fig. 6b).
(2) The hydrothermal zircons are 50–100 μm in size, and the $^{206}Pb/^{238}U$ age of these zircons is much younger than that of the basaltic zircons, ranging from 226.5 to 79.7 Ma; their $f^{206}Pb\%$ value is higher than that of the basaltic zircons, ranging from 0.43 to 18.2. These zircons have relatively low contents of Th (21–460 ppm) and U (11–1163 ppm), with Th/U ratios ranging from 0.15 to 2.03. Half of the zircon grains

Table 2
U–Pb isotopic compositions for zircon from the Gejiu basalt sample XSDI.

Sample	U (ppm)	Th (ppm)	Th/U Ratio	$f_{206}\%$	$^{207}Pb/^{206}Pb$ Ratio	σ (%)	$^{207}Pb/^{235}U$ Ratio	σ (%)	$^{206}Pb/^{238}U$ Ratio	σ (%)	$^{206}Pb/^{238}U$ Age (Ma)	σ (Ma)
Basaltic zircons												
XSDI@18	818	226	0.28	0.24	0.05184	1.86	0.28344	2.77	0.0411	1.52	259.9	3.9
XSDI@2	715	173	0.24	0.08	0.05296	1.59	0.291	2.32	0.0403	1.55	254.9	3.9
XSDI@25	440	267	0.61	0.24	0.05028	2.12	0.26518	3.1	0.0397	1.51	251.1	3.7
XSDI@17	405	220	0.54	0.13	0.05104	2.65	0.27324	3.3	0.0396	1.51	250.4	3.7
XSDI@16	1416	292	0.21	0.41	0.05563	1.36	0.28513	2.53	0.0395	1.5	249.6	3.7
XSDI@20	521	340	0.65	2.79	0.07278	1.96	0.27558	5.89	0.0393	1.52	248.6	3.7
XSDI@30	678	180	0.27	0.05	0.05172	2.46	0.27809	2.95	0.0393	1.52	248.4	3.7
XSDI@19	770	582	0.76	0.09	0.05131	1.58	0.27376	2.31	0.0392	1.5	248.1	3.7
XSDI@22	360	232	0.64	3.4	0.08257	1.91	0.2996	6.8	0.0388	1.53	245.2	3.7
XSDI@29	1039	1142	1.10	0.36	0.05282	2	0.26541	2.91	0.0385	1.53	243.7	3.7
XSDI@3	691	231	0.33	0.08	0.05146	1.53	0.26945	2.32	0.0385	1.5	243.3	3.6
XSDI@13	256	105	0.41	0.12	0.04994	2.63	0.25927	3.41	0.0384	1.61	242.8	3.8
XSDI@21	462	305	0.66	0.18	0.0508	2.04	0.25989	2.96	0.0382	1.5	241.6	3.6
XSDI@32	499	351	0.70	0.12	0.05473	1.95	0.28145	2.62	0.038	1.5	240.3	3.5
XSDI@1	571	109	0.19	0.21	0.05076	1.77	0.25598	2.7	0.0378	1.57	239.4	3.7
XSDI@4	501	282	0.56	0.11	0.05111	1.87	0.26194	2.59	0.0378	1.51	239.4	3.6
XSDI@23	458	293	0.64	2.18	0.06363	2.2	0.24182	8.2	0.0378	1.55	239.2	3.6
XSDI@24	848	775	0.91	0.19	0.05261	2.18	0.26602	2.93	0.0378	1.51	238.9	3.5
XSDI@28	672	224	0.33	0.09	0.05036	1.87	0.25834	2.56	0.0377	1.51	238.8	3.5
XSDI@9	565	135	0.24	0	0.05284	1.74	0.27351	2.31	0.0375	1.52	237.6	3.5
XSDI@26	409	233	0.57	0.74	0.05667	2.17	0.26273	5.13	0.0375	1.52	237.2	3.5
Hydrothermal zircons												
XSDI@10*	1163	171	0.15	0.43	0.05334	1.19	0.24617	2.52	0.0358	1.5	226.5	3.3
XSDI@27*	718	176	0.25	0.63	0.05153	1.82	0.20917	3.45	0.0326	1.55	206.6	3.1
XSDI@31*	555	167	0.30	1.16	0.05413	2.2	0.17702	6.83	0.0286	1.54	181.6	2.8
XSDI@11*	239	210	0.88	3.78	0.05202	5.25	–	–	0.0154	1.76	98.5	1.7
XSDI@14	258	59	0.23	1.87	0.05739	5.53	0.07918	13.59	0.0135	1.71	86.3	1.5
XSDI@7	89	35	0.39	5.96	0.06252	6.75	–	–	0.0131	2.62	83.9	2.2
XSDI@12	151	67	0.44	2.26	0.07071	4.61	0.09277	13.07	0.0127	1.64	81.3	1.3
XSDI@5*	11	21	2.03	18.2	0.07911	16.38	–	–	0.0126	9.14	80.5	7.3
XSDI@6	284	460	1.62	0.77	0.04811	5.7	0.07211	9.42	0.0125	1.61	79.8	1.3
XSDI@8	226	71	0.31	11.9	0.06526	6.37	–	–	0.0123	2.57	78.7	2
Inherited zircon												
XSDI@15*	147	78	0.53	0.55	0.09071	1.12	2.56313	2.15	0.2147	1.5	1253.7	17.1

Note: $f^{206}Pb\%$ is (common ^{206}Pb / total^{206}Pb) × 100; the sample with * is not used for the weighted mean $^{206}Pb/^{238}U$ age calculation.

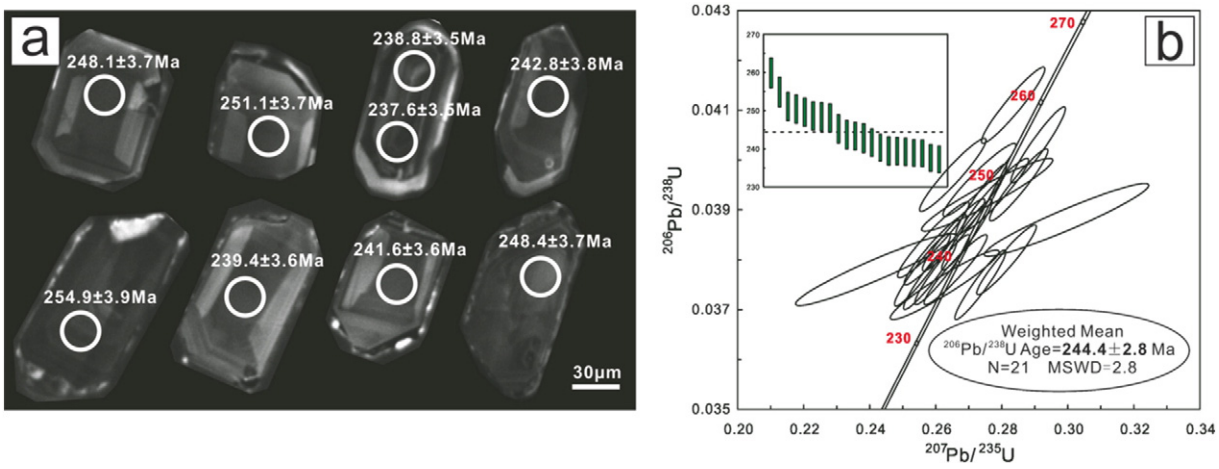

Fig. 6. (a) Cathodoluminescence images for the basaltic zircons from sample XSDI for SIMS dating. (b) U–Pb concordia plots showing results of SIMS dating of zircons.

(5 in 10) fall within a single population with a weighted mean $^{206}Pb/^{238}U$ age of 81.9 ± 3.7 Ma (MSWD = 3.7).

(3) The inherited zircon, spot XSDI@15 with a $^{206}Pb/^{238}U$ age of 1254 ± 17 Ma, is the oldest zircon. The inherited zircon is normally found within the basaltic magma in the Gejiu–Kaiyuan district (Zhang et al., 2013).

5.2. Major and trace element compositions

The whole-rock major and trace element compositions (normalized to 100 wt.% anhydrous) and the CIPW norm calculation are reported in Supplementary Table S1.

5.2.1. The KF basalt

All of the KF basalts plot in the field of alkaline basalt in the Zr/Ti vs Nb/Y diagram (Fig. 7a) of Winchester and Floyd (1977) and revised by Pearce (1996), which may be used to classify the rocks according to their alkalinity and stage of differentiation using immobile elements. The TiO_2 contents have a small range from 2.28 to 2.88 wt.%. The KF basalt contains extraordinarily high levels of MgO (9.63–20.8 wt.%) and lower SiO_2 (40.2–46.5 wt.%) compared with the LC and QLS basalts. The KF basalt contains higher amounts of K_2O (1.26–6.94 wt.%) than Na_2O (0.31–1.74 wt.%), with K/Na ratios far greater than 1 (Fig. 7b).

The KF basalt has strongly positive Rb (as high as 2140 ppm) and K anomalies, slight Pb anomalies, and variable Sr contents but is devoid of any Eu anomalies. The $(La/Yb)_N$ values (primitive-mantle-normalized using data from Sun and McDonough, 1989) range from 8.51 to 13.9. Both in the primitive-mantle-normalized trace element diagram (Fig. 8a) and in the chondrite-normalized rare earth element (REE) diagram (Fig. 8b), the KF basalt displays patterns of enrichment in the large-ion lithophile elements (LILE) relative to the high field strength elements (HFSE). Furthermore, the patterns are similar to those of the Kaiyuan basalt reported by Zhang et al. (2013).

5.2.2. The LC basalt

The LC basalt is alkaline in composition (Fig. 7a). The basalt is characterized by high MgO (10.3–14.4 wt.%) and a small range of SiO_2 (45.8–47.1 wt.%) concentrations. The TiO_2 concentrations range from 2.59 to 3.26 wt.%. The LC basalt contains more K_2O (0.87–4.60 wt.%) than Na_2O (0.63–2.03 wt.%), with K/Na ratios greater than 1 (Fig. 7b).

The LC basalt has positive Rb (as high as 784 ppm) and K and Pb anomalies, but lacks any Eu anomaly. It is enriched in LREE and has $(La/Yb)_N$ values ranging from 10.8 to 17.5. The patterns of the QLS basalt are similar to those of the Kaiyuan basalt on the primitive-mantle-normalized trace element diagram (Fig. 8c) and the chondrite-normalized REE diagram (Fig. 8d).

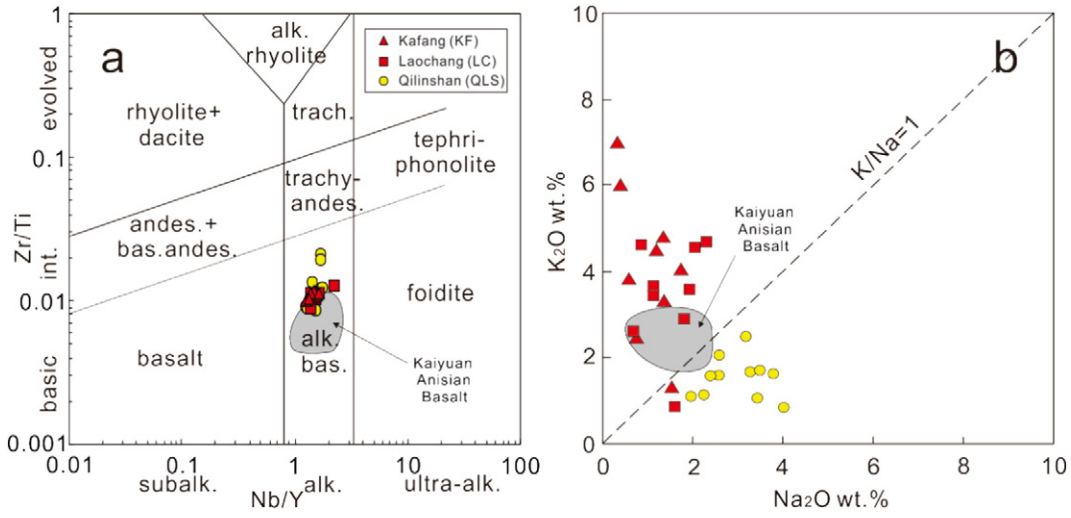

Fig. 7. (a) Zr/Ti vs. Nb/Y classification diagram. (b) Na_2O vs K_2O diagram.

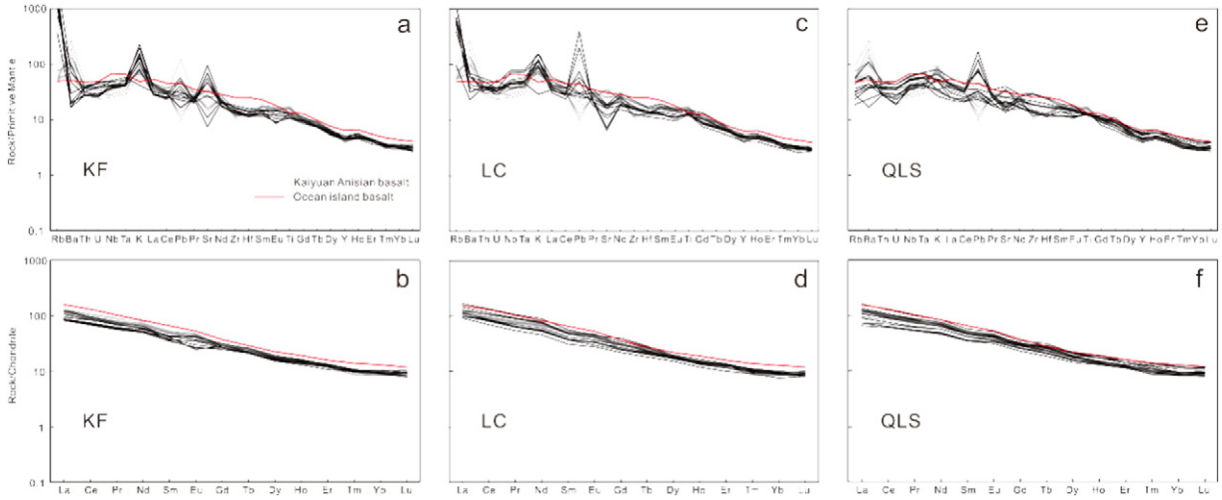

Fig. 8. Primitive-mantle-normalized trace element patterns and chondrite-normalized REE patterns of the Gejiu basalts. Normalization and ocean island basalts (red line) values followed Sun and McDonough (1989).

5.2.3. The QLS basalt

The QLS basalts correlate with the alkaline basalt in the Zr/Ti vs Nb/Y diagram (Fig. 7a). The QLS basalts are characterized by high SiO_2 (45.3–48.7 wt.%) and TiO_2 (2.59–3.08 wt.%) and low MgO (7.49–11.3 wt.%) concentrations compared with the KF and LC basalts. In contrast with the KF and LC basalts, the QLS basalt contains more Na_2O (1.91–3.98 wt.%) than K_2O (0.84–2.49 wt.%), with K/Na ratios of less than 1 (Fig. 7b).

The QLS basalt is enriched in LILE relative to HFSE, with strongly positive Pb anomalies and no obvious Rb (11.8–35.3 ppm) or K anomalies. The rocks have $(La/Yb)_N$ ratios from 7.62 to 17.86 and mildly positive Eu anomalies. The patterns of the QLS basalt are similar to those of the Kaiyuan basalt on the primitive-mantle-normalized trace element diagram (Fig. 8e) and the chondrite-normalized REE diagram (Fig. 8f).

5.3. Sr and Nd isotopic compositions

The $^{87}Sr/^{86}Sr$ and $^{143}Nd/^{144}Nd$ ratios of selected samples are listed in Table 3. The initial isotopic ratios were corrected to a nominal age of 244 Ma. All of the analyzed QLS basalts have variable positive $\varepsilon Nd(t)$ values ranging from 0.6 to 2.5 and uniform $(^{87}Sr/^{86}Sr)_i$ values ranging from 0.7042 to 0.7049. The plots of the Sr–Nd isotopic compositions indicate a negative correlation between the compositions of the QLS basalts and the mantle array, similar to the Kaiyuan basalt and overlapping with that of the Emeishan flood basalt (Wang et al., 2007).

5.4. Pb isotopic compositions

The Pb isotopic compositions of the Gejiu basalts of this study and of the ore from the Kafang deposit in the literature are presented in Table 4. The KF and QLS basalts have a $^{206}Pb/^{204}Pb$ range from 18.930 to 19.001, a $^{207}Pb/^{204}Pb$ range from 15.592 to 15.708, and a $^{208}Pb/^{204}Pb$ range from 38.670 to 39.527. The initial isotopic ratios were corrected to nominal ages of 244 and 84 Ma, respectively. The $(^{206}Pb/^{204}Pb)_{244\ Ma}$ values range from 17.475 to 18.214, the $(^{207}Pb/^{204}Pb)_{244\ Ma}$ values range from 15.539 to 15.699, and the $(^{208}Pb/^{204}Pb)_{244\ Ma}$ values range from 37.557 to 38.432; the $(^{206}Pb/^{204}Pb)_{84\ Ma}$ values range from 18.307 to 18.562, the $(^{207}Pb/^{204}Pb)_{84\ Ma}$ values range from 15.576 to 15.705, and the $(^{208}Pb/^{204}Pb)_{84\ Ma}$ values range from 38.484 to 39.038.

5.5. S isotopic compositions

The S isotopic compositions are reported in Table 5. The 23 samples of this study and the 14 samples from the literature covered all of the S isotopic compositions of the Kafang deposit. The $\delta^{34}S$ values have a Gaussian distribution; small variations are exhibited, yielding positive $\delta^{34}S$ values in the range of 1.51 to 5.11‰.

6. Discussion

6.1. Onset of magmatism and mineralization

6.1.1. Eruption and alteration ages of the Gejiu basalts

According to Xue (2002), YBGMR (1982), and Zhang et al. (2014), the basalts emplaced into the Gejiu Formation have been discovered at Kafang, Laochang, and Qilinshan in the Gejiu district and at Dongliancun and Bapanzhai in the Kaiyuan district (Fig. 1b). The zircon geochronology study suggests that the Gejiu basalts were erupted at 244.4 ± 2.8 Ma. This age is consistent with the age of the Kaiyuan basalt (247.7 ± 1.7 Ma) within uncertainty and is also consistent with the age of the Gejiu Formation (245–237 Ma). Thus, our data confirm that the age of basaltic magmatism is constrained between 247.7 and 244.4 Ma.

The zircon geochronology also records a hydrothermal event with an age of 81.9 ± 3.7 Ma. Phlogopite abounds in the KF and LC basalts (e.g., Wang, 1993), and Zhang et al. (2012a) reported a phlogopite

Table 3
Sr–Nd isotopic compositions of QLS basalt.

Sample	Rb	Sr	$^{87}Sr/^{86}Sr$	σ	$(^{87}Sr/^{86}Sr)_i$	Sm	Nd	$^{143}Nd/^{144}Nd$	σ	$(^{143}Nd/^{144}Nd)_i$	$\varepsilon Nd(t)$
QLS-6	35.3	829	0.704677	4	0.70424	8.45	38.1	0.512665	2	0.512447	2.5
QLS-7	20.5	389	0.705195	5	0.70466	7.30	32.1	0.512611	2	0.512388	1.4
QLS-8	18.1	354	0.705405	7	0.70488	7.73	34.9	0.512637	2	0.512419	2.0
QLS-9	19.6	349	0.705411	6	0.70484	6.86	29.0	0.512589	4	0.512357	0.7
QLS-10	27.8	515	0.705000	7	0.70445	7.04	31.1	0.512615	3	0.512392	1.4
QLS-11	14.9	312	0.705228	4	0.70474	6.99	29.3	0.512582	1	0.512348	0.6

Note: $(^{87}Sr/^{86}Sr)_i$, $(^{143}Nd/^{144}Nd)_i$ and $\varepsilon Nd(t)$ were calculated for 244 Ma.

Table 4
Pb isotopic compositions of the Gejiu basalt and the Kafang stratiform Cu deposit.

Sample	Location	Mineral	$^{206}Pb/^{204}Pb$	2σ	$^{207}Pb/^{204}Pb$	2σ	$^{208}Pb/^{204}Pb$	2σ	Reference
KF-5	Kafang Qianjin adit	Basalt bulk powder	19.001	0.003	15.697	0.003	39.527	0.007	This study
KF-8	Kafang Qianjin adit	Basalt bulk powder	19.001	0.003	15.683	0.002	39.386	0.006	This study
KF-9	Kafang Qianjin adit	Basalt bulk powder	18.608	0.003	15.668	0.002	39.073	0.006	This study
QLS-6	N 23°19′16.4″, E 103°17′3.8″	Basalt bulk powder	18.637	0.001	15.611	0.001	38.981	0.003	This study
QLS-7	N 23°19′16.4″, E 103°17′3.8″	Basalt bulk powder	18.39	0.002	15.708	0.002	38.67	0.004	This study
QLS-8	N 23°19′16.4″, E 103°17′3.8″	Basalt bulk powder	18.651	0.002	15.592	0.002	38.947	0.005	This study
QLS-9	N 23°19′16.4″, E 103°17′3.8″	Basalt bulk powder	18.528	0.003	15.608	0.002	38.812	0.005	This study
QLS-10	N 23°19′16.4″, E 103°17′3.8″	Basalt bulk powder	18.474	0.002	15.614	0.002	38.707	0.004	This study
QLS-11	N 23°19′16.4″, E 103°17′3.8″	Basalt bulk powder	18.477	0.002	15.622	0.002	38.731	0.004	This study
QJK-16CP	Kafang 1820 adit	Chalcopyrite	18.253		15.553		38.155		Yang et al. (2010)
QJK-29CP	Kafang 1870 adit	Pyrrhotite	18.214		15.533		38.045		Yang et al. (2010)
QJK-16PR	Longshujiao	Pyrrhotite	18.315		15.59		38.36		Yang et al. (2010)
DGL-16PR	Donggualin 1640 adit	Pyrrhotite	18.443		15.626		38.568		Yang et al. (2010)
DGL-15CP	Donggualin 1640 adit	Chalcopyrite	18.556		15.666		38.773		Yang et al. (2010)
DGL-7PR	Donggualin 1690 adit	Pyrrhotite	18.447		15.65		38.717		Yang et al. (2010)
JZL-2CP	Jinzhulin 2055 adit	Chalcopyrite	18.516		15.666		38.844		Yang et al. (2010)

^{40}Ar–^{39}Ar plateau age of 85.0 ± 0.6 Ma for the KF basalt. The hydrothermal zircon age and the ^{40}Ar–^{39}Ar altered age of the KF basalt are consistent with the magmatic zircon U–Pb age (85.5–83.3 Ma) of the Cretaceous granite reported by Cheng and Mao (2010). Accordingly, the alteration process of the KF basalts is temporally related to the emplacement of the Cretaceous granite.

6.1.2. Mineralization age of the Kafang deposit

The Anisian basalts are widely spread throughout the Gejiu and Kaiyuan districts. If the mineralization is synchronous with the basalts, all of the basalts should be enriched in Cu. The Cu contents of KF basalt range from 370 to 3460 ppm. However, the average Cu contents of QLS basalt (47 ppm) in the Gejiu district and the Kaiyuan basalt (85 ppm) are very low. In the Gejiu district, Cu mineralization has only been observed in the KF and LC basalts. The chalcopyrite and pyrrhotite show an alternating layer structure in hand specimen, and euhedral to subhedral granular texture under the microscope, which implies that chalcopyrite and pyrrhotite formed simultaneously. The pyrrhotite filled the amygdales (Fig. 3b), indicating that sulfide mineralization occurred later than the eruption of the basalt. Most importantly, no

Table 5
S isotopic compositions of the Kafang stratiform Cu deposit.

Sample	Location	Mineral	$\delta^{34}S_{V\text{-}CDT}$ (‰)	SD	Reference
11KF-34G	Kafang 1820 adit I-9-3	Chalcopyrite	1.96	0.04	This study
11KF-34F	Kafang 1820 adit I-9-3	Chalcopyrite	1.83	0.05	This study
11KF-34F	Kafang 1820 adit I-9-3	Pyrrhotite	1.70	0.01	This study
11KF-34D	Kafang 1820 adit I-9-3	Chalcopyrite	1.70	0.00	This study
11KF-34D	Kafang 1820 adit I-9-3	Pyrrhotite	1.78	0.01	This study
11KF-34A	Kafang 1820 adit I-9-3	Chalcopyrite	3.34	0.04	This study
11KF-34A	Kafang 1820 adit I-9-3	Pyrrhotite	3.33	0.01	This study
11KF-28H	Kafang 1820 adit 15-2-1	Chalcopyrite	2.74	0.04	This study
11KF-28G	Kafang 1820 adit 15-2-1	Chalcopyrite	2.62	0.00	This study
11KF-28G	Kafang 1820 adit 15-2-1	Pyrrhotite	2.06	0.01	This study
11KF-28F	Kafang 1820 adit 15-2-1	Pyrrhotite	4.34	0.03	This study
11KF-25E	Kafang 1820 adit 15-2-1	Chalcopyrite	1.61	0.03	This study
11KF-25E	Kafang 1820 adit 15-2-1	Pyrrhotite	1.51	0.06	This study
11KF-19G	Kafang Qianjin adit	Chalcopyrite	4.68	0.03	This study
11KF-19G	Kafang Qianjin adit	Pyrrhotite	4.59	0.04	This study
11KF-19F	Kafang Qianjin adit	Chalcopyrite	4.76	0.00	This study
11KF-19F	Kafang Qianjin adit	Pyrrhotite	4.61	0.13	This study
11KF-19D	Kafang Qianjin adit	Chalcopyrite	5.11	0.03	This study
11KF-19D	Kafang Qianjin adit	Pyrrhotite	4.95	0.10	This study
11KF-19B	Kafang Qianjin adit	Chalcopyrite	4.62	0.08	This study
11KF-19A	Kafang Qianjin adit	Chalcopyrite	4.74	0.01	This study
09KF-6-1	Kafang Qianjin adit	Pyrrhotite	4.06	0.00	This study
09KF-6-2	Kafang Qianjin adit	Chalcopyrite	4.11	0.01	This study
QJK-16CP	Kafang Qianjin adit	Chalcopyrite	1.5	–	Cheng et al. (2012)
QJK-10CP	Kafang Qianjin adit	Chalcopyrite	1.5	–	Cheng et al. (2012)
QJK-43CP	Kafang Qianjin adit	Chalcopyrite	2.9	–	Cheng et al. (2012)
QJK-29CP	Kafang Qianjin adit	Chalcopyrite	2.6	–	Cheng et al. (2012)
QJK-3CP	Kafang Qianjin adit	Chalcopyrite	2.3	–	Cheng et al. (2012)
QJK-16PR	Kafang Qianjin adit	Pyrrhotite	2.8	–	Cheng et al. (2012)
S20	Kafang Qianjin adit	Chalcopyrite	3.3	–	Qin and Li (2008)
S21	Kafang Qianjin adit	Chalcopyrite	−1.4	–	Qin and Li (2008)
S31-1	Jinguangpo 1820 adit	Pyrrhotite	2.6	–	Qin and Li (2008)
S31-2	Jinguangpo 1820 adit	Pyrrhotite	−1.8	–	Qin and Li (2008)
S33	Jinguangpo 1820 adit	Chalcopyrite	1.3	–	Qin and Li (2008)
S35	Kafang Qianjin adit	Chalcopyrite	−0.9	–	Qin and Li (2008)
S38	Kafang Qianjin adit	Chalcopyrite	3.1	–	Qin and Li (2008)
S40	Kafang Qianjin adit	Chalcopyrite	−0.9	–	Qin and Li (2008)

Note: SD = standard deviation.

mineralization age has been reported to support the synchronous occurrence of the basalt and the stratiform ore.

Cheng et al. (2012) obtained a Re–Os isochronal age for molybdenite samples of 84.2 ± 7.3 Ma from the Kafang stratiform Cu ore, which is interpreted as representing the age of stratiform Cu ore hosted by basalt. Zhang et al. (2012b) discovered that phlogopite coexists with chalcopyrite and pyrrhotite in the Kafang stratiform Cu ore. The ^{40}Ar–^{39}Ar plateau age of phlogopite is 79.6 ± 0.5 Ma. Therefore, the Cu mineralization (84.2–79.6 Ma) of the basalt was synchronous in the Late Cretaceous, with the granite emplacement (85.5–83.3 Ma) and alteration process (85.0–81.9 Ma). These pieces of evidence indicate that the basalt-hosted stratiform Cu ore is temporally related to the granite.

6.2. Source of ore-forming material

As shown in Fig. 9, Pb isotope compositions of the stratiform ore are similar to those of the Gejiu basalts but distinctly different from those of the granite. These features indicate that the ore-forming material of the stratiform ore may have originated from the basalt. The unaltered basalt has an average Cu content ranging from 47 ppm (QLS basalt) to 85 ppm (Kaiyuan basalt). The average Cu content of granite is 9.84 ppm, which is much less than the Cu content in the Gejiu basalts. Assuming that the volume of the Gejiu basalts is 21×10^8 m^3 (Cheng, 2012), the mass density of the basalt is 3.0 t/m^3. This is sufficient to provide at least 0.3–0.55 Mt of Cu, which is in accordance with the Cu reserve of the Kafang deposit (0.4 Mt).

Ores from the Kafang deposit are mainly represented by chalcopyrite and pyrrhotite. The lack of sulfate minerals in the ore suggests that the $\delta^{34}S$ value of sulfide can essentially represent the total S isotope composition of the hydrothermal fluid, i.e., $\delta^{34}S_{\sum S} \approx \delta^{34}S$ sulfide (Ohmoto, 1972). Our results and previous results show $\delta^{34}S$ values ranging from −1.8‰ to 5.1‰ for basalt-hosted stratiform Cu ore (Fig. 10a). The $\delta^{34}S$ values of the stratiform ore are compatible with the range of sulfur (0‰–5‰) in basalt, either directly from an igneous source or obtained by leaching of sulfur-bearing minerals in igneous rocks (e.g., Ohmoto, 1986). Furthermore, they are also close to the range of sulfur in the Gejiu basalt (2.6‰–3.8‰) but significantly different from that of granite $\delta^{34}S$ values (−3.7‰–0.1‰) and the Gejiu Formation $\delta^{34}S$ values (7.1‰–11.1‰) (Cheng et al., 2012), as evident from Fig. 10b. Based on the report by Zhang et al. (2014), the unaltered basalt has an average S content ranging from 174 ppm (Kaiyuan basalt) to 229 ppm (QLS basalt). Thus, the Gejiu basalts could provide sulfur for ore-forming fluid.

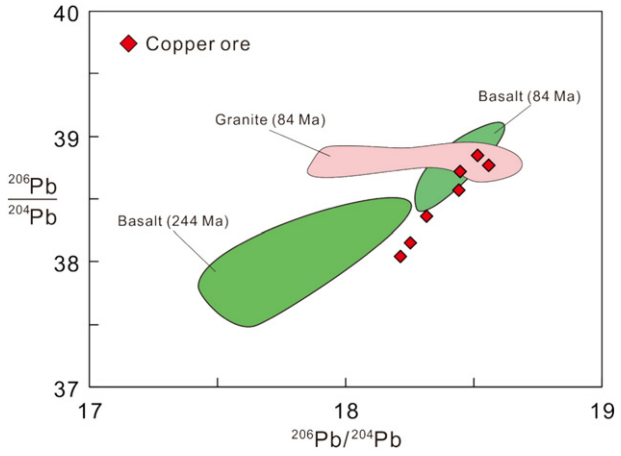

Fig. 9. Diagram of Pb isotope compositions of the Gejiu basalts (whose initial isotopic ratios were corrected to nominal ages of 244 and 84 Ma), Gejiu granite (using data from unpublished results and corrected to a nominal age of 84 Ma), and the Kafang stratiform Cu deposit.

Based on the Pb and S isotopic characteristics, we conclude that the ore-forming materials in the Kafang deposit are directly obtained from the basalt.

6.3. Petrogenesis of the Gejiu basalts

6.3.1. Alteration-induced K and Mg anomalies

Rubidium (Rb) is an alkali element (Group 1), and similar to other alkalis, it is generally very soluble in water and hydrous fluid. As a result, Rb is readily transported in solution and able to move into or out of rock alteration systems (e.g., Rollinson, 1993). The concentration of Rb in ocean island basalts (OIB) is only 31 ppm (Sun and McDonough, 1989). The concentrations of Rb in the Gejiu basalts are ranked as follows: QLS basalt (11.8–35.3 ppm) < LC basalt (60.8–784 ppm) < KF basalt (234–2140 ppm). It is difficult to conceive of a process of magmatic evolution responsible for such variation in the Rb concentrations in the KF and LC basalts. More likely, this variation is the result of alteration.

As evident in Fig. 11a and b, the Rb concentration (used as an alteration index because of its geochemical character) may provide three indications of the alteration of the Gejiu basalts: (1) The alteration caused the increased K_2O and decreased Na_2O concentrations in the Gejiu basalts; (2) the KF, LC, and QLS basalts have undergone extreme, intermediate, and weak alteration, respectively; and (3) despite the weathering, the QLS basalts were closest in composition to the parental magma of the Gejiu basalts.

There are two possible ways to increase the amount of K in rock: (1) simultaneous basalt–seawater exchange reactions (e.g., Hart, 1969) or (2) a process of deuteric hydrothermal alteration (e.g., Páez et al., 2010). If the increased K_2O amounts are attributed to simultaneous basalt–seawater exchange reactions, the K_2O concentrations of the QLS basalt should be correspondingly high. However, the QLS basalt has the lowest concentrations of K_2O (0.84–2.49 wt.%) among the Gejiu basalts. Consequently, the first explanation may be ruled out.

Cheng et al. (2012) suggest that all the ore-forming fluids of the entire Kafang deposit were derived from the granite. The hydrothermal zircon U–Pb age and the phlogopite ^{40}Ar–^{39}Ar plateau age for the KF basalt are consistent with the zircon U–Pb age of the granite, indicating that the alteration of the KF and LC basalts was temporally related to the emplacement of the granite. Whole-rock analyses indicate that the granite is high in K and alkali (Cheng and Mao, 2010), and the fluid inclusions in quartz and calcite, which represent the Kafang stratiform Cu ore, show that the average salinities of the inclusions were from 11.0 to 22.6 wt.% NaCl equiv. (Cheng et al., 2012). Because the KF and LC basalts are in contact with the granite (Figs. 2 and 3), the basalt may have undergone intense granite-related hydrothermal alteration. Correspondingly, the amounts of K and Rb in the KF and LC basalts increased dramatically. The QLS basalt is located several hundred meters from the granite, and the Kaiyuan basalt is 50 km away from the Gejiu district, so these basalts were much less altered than the KF and LC basalts.

The average concentration of MgO in the KF and LC basalts (13.3 wt.%) is higher than those of rocks of the same type, such as Emeishan high Ti basalt (5.21 wt.%, reported by Wang et al., 2007), and some samples had extraordinarily high levels of MgO (e.g., KF-5 and KF-7). However, based on the classification and nomenclature of picrites (Le Bas, 2000), none of the Gejiu basalts can be classified as picrites. This is because the diagram can be used only if the MgO and $Na_2O + K_2O$ constituents are essentially primary. The granite is poor in MgO, and thus the Mg was derived from a different source. Triassic dolomite is widespread and constitutes the country rock around both the basalt and granite, and it is enriched in MgO (average of 14.8 wt.%, unpublished result). It is therefore possible that, when the hydrothermal fluid passed through the dolomite, it transported the Mg and finally moved Mg into the basalt. Therefore, we suggest that the Mg in basalt is gained from dolomite by the transportation of granite-related hydrothermal fluid.

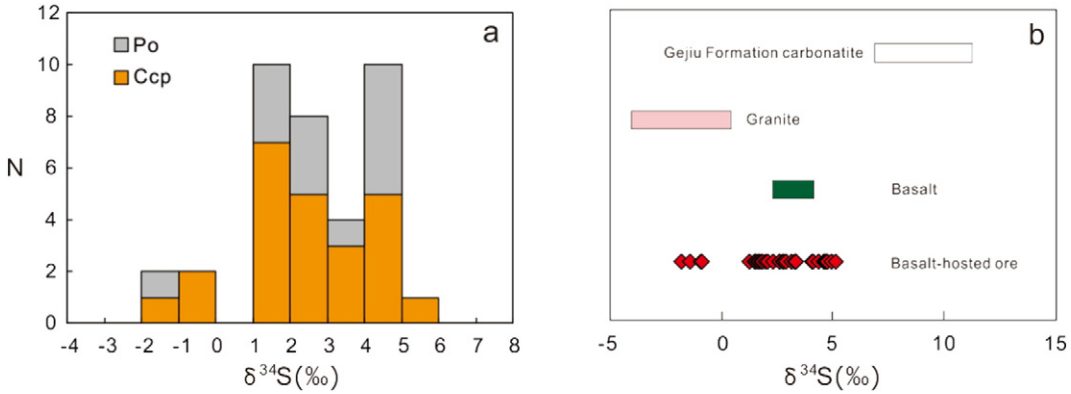

Fig. 10. (a) S isotopic composition histogram of the Kafang stratiform Cu deposit. (b) S isotope distribution of the different units of the Kafang stratiform Cu deposit. The isotopic compositions of Gejiu Formation carbonates, granite, and basalt followed Cheng et al. (2012).

During the period 85.5–83.3 Ma, granite intruded into the Gejiu Formation, and the KF and LC basalts underwent intense granite-related hydrothermal alteration, which changed the major element compositions of the KF and LC basalts. Major minerals in basalt such as olivine, pyroxene, and albite will alter to minerals such as phlogopite and chlorite with reactions (after Lu, 2008) as follows:

$$3(Mg,Fe)_2[SiO_4](\text{olivine}) + 2\,K^+ + 3SiO_2 + Al_2O_3 + 3H_2O \rightarrow 2K(Mg,Fe)_3[AlSi_3O_{10}](OH)_2(\text{phlogopite}) + 2H^+,$$

$$Ca(Mg,Fe)Si_2O_6(\text{pyroxene}) + 2K^+ + 5Mg^{2+} + 5Fe^{3+} + Al_2O_3 + 4SiO_2 + HCO_3^- + 7H_2O \rightarrow 2K(Mg,Fe)_3[AlSi_3O_{10}](OH)_2(\text{phlogopite}) + CaCO_3 + 11H^+,$$

$$2NaAlSi_3O_8(\text{Albite}) + 4(Mg,Fe)^{2+} + 2(Fe,Al)^{3+} + 10H_2O \rightarrow (Mg,Fe)_4(Fe,Al)_2Si_2O_{10}(OH)_8(\text{chlorite}) + 4SiO_2 + 2Na^+ + 12H^+.$$

These reactions resulted in the formation of minerals rich in K and Mg (such as phlogopite) and thus increased the levels of K_2O and MgO in the basalt.

6.3.2. Tectonic setting and mantle source of the Gejiu basalts

The KF and LC basalts had undergone pervasive alteration. The QLS basalt was subjected to intense weathering. However, the linear correlations between La and the other REE and HFSE (Fig. 11c and d), and the consistent ratios between these elements, indicate that the HFSE and REE were relatively immobile during the alteration and weathering processes. This is consistent with the previous demonstration that HFSE and REE are resistant during those processes (Staudigel and Hart, 1983; Wang et al., 2007). Accordingly, the concentrations of HFSE and REE reported here are assumed to be suitable proxies for evaluating the petrogenesis of the Gejiu basalts.

Several diagrams may be used for the tectonic discrimination of basaltic lava erupted in the majority of tectonic environments (Meschede, 1986; Pearce and Cann, 1973; Wood, 1980). The Nb–Zr–Y (Fig. 12a), Ti–Zr–Y (Fig. 12b), and Hf–Th–Ta (Fig. 12c) diagrams all imply that the Gejiu basalts are intraplate basalts (OIB and continental flood basalts). This intraplate environment was also supported by the paleogeographic reconstructions of Metcalfe (2006).

The Gejiu basalts are situated within the Emeishan Large Igneous Province (ELIP) district and are present in the Gejiu Formation. They exhibit LREE-enriched patterns (Fig. 8) and OIB-like incompatible element ratios (Fig. 13). The QLS basalt has Sr–Nd isotope ratios similar to those of the Emeishan flood basalt (Fig. 13c) and all of the Gejiu basalts in the Emeishan high-Ti basalt district as evident from Fig. 13d. Zhang et al. (2014) found that the palladium-group PGE (Rh, Pd, Pt) contents of basalt

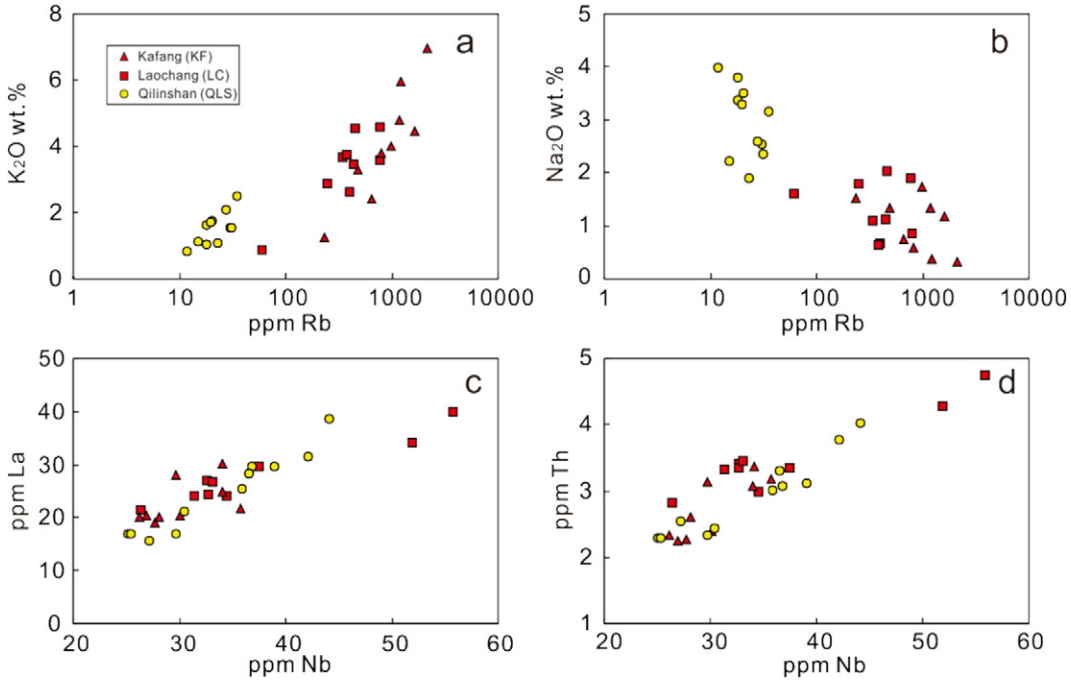

Fig. 11. Variation diagrams of the Gejiu basalts: (a) Rb vs K_2O, (b) Rb vs Na_2O, (c) Nb vs La, and (d) Nb vs Th.

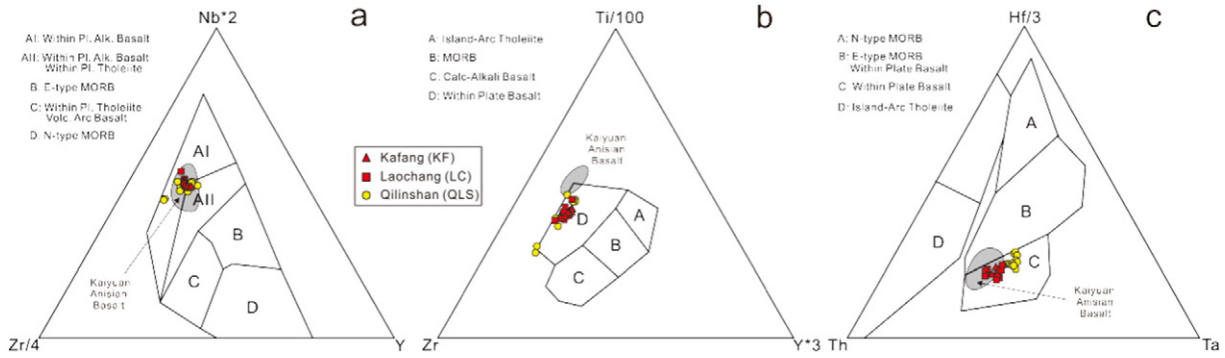

Fig. 12. Tectonic setting discrimination diagrams for the Gejiu basalts: (a) Nb–Zr–Y diagram (Meschede, 1986), (b) Ti–Zr–Y diagram (Pearce and Cann, 1973), and (c) Hf–Th–Ta diagram (Wood, 1980).

are markedly depleted compared with the Emeishan high Ti basalt, which is caused by the early extraction of PPGE during the eruption of the Emeishan basalt. Because of its younger eruption age (244.4 Ma) compared with that of the Emeishan plume main event (260–257 Ma), the Gejiu basalts may represent a volcanic series involving remelting of the Emeishan plume head owing to the post-Emeishan large igneous province stress relaxation of the Yangtze craton after the main Emeishan plume event.

6.4. A possible genetic model

VMS deposits are accumulations of sulfide minerals that precipitated at or near the seafloor in spatial, temporal, and genetic association with contemporaneous volcanism (Franklin et al., 1981; Barrie and Hannington, 1999; Large et al., 2001). VMS deposits consist of a concordant massive sulfide lens and discordant vein-type sulfide mineralization located in the footwall rocks. VMS deposits are associated with bimodal basalt–rhyolite magmatism (e.g., Wyman, 2000; Hart et al., 2004). Petrochemically, the basalt is similar to oceanic and continental arc basalt. For example, Swinden (1991), using petrochemistry of the Ordovician mafic volcanic rocks in Newfoundland, demonstrated the propensity for VMS deposits to form in proto-arc and rifted-arc terranes. The tectonics of VMS deposits are related either to ocean–ocean subduction, which represents an evolution from nascent arc rifting to mature back-arc development, or to ocean–continent margin to continental back-arc environments. The dominant ore-forming fluid is modified seawater, which carries the metals and sulfur. Most importantly, the VMS deposits are synchronous with the basalt and its hydrothermal system (Franklin et al., 2005, and the references within).

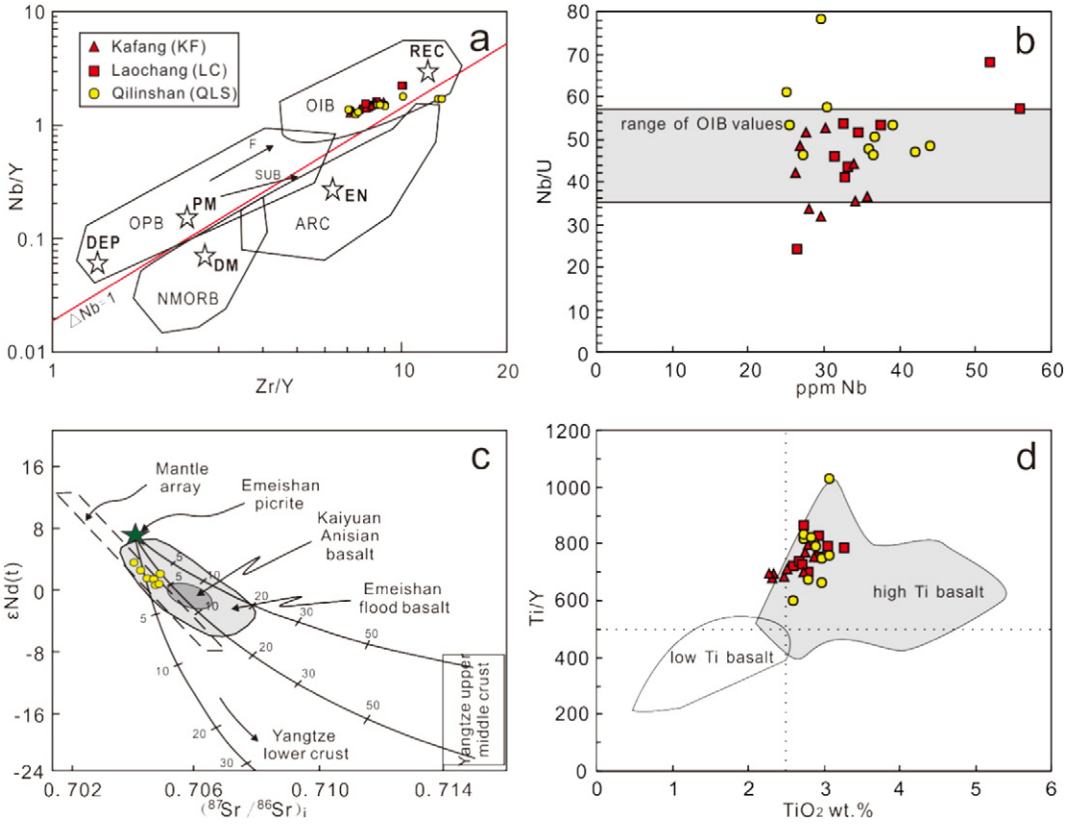

Fig. 13. (a) Zr/Y–Nb/Y diagram (Condie, 2003) showing mantle compositional components and fields for basalts from various tectonic settings. Arrows indicate the effects of batch melting (F) and subduction (SUB). (b) Nb/U vs Nb (ppm) plot. OIB values are from Hofmann et al. (1986). (c) εNd(t) (t = 244 Ma) values vs initial $^{87}Sr/^{86}Sr$ diagram for the Gejiu basalts (modified after Wang et al., 2007). The numbers indicate the percentages of participation of the crustal materials. (d) Ti/Y vs TiO_2 plot used for the subdivision of the Emeishan basalts into high-Ti and low-Ti basalts based on Shellnutt and Jahn (2011).

The Kafang stratiform Cu deposit differs markedly from the VMS-type deposits in several important respects. The Kafang deposit does not develop vein-type ore bodies. The volcanism has OIB characteristics. The tectonic setting of the basalt is within the plate. The dominant fluid in the Kafang deposit is magmatic, and the metals and sulfur are derived from the basalt. The formation of the basalt is temporally inconsistent with the Cu mineralization and hydrothermal alteration. More importantly, Cheng et al. (2012, 2013) reported the precise granite emplacement age and the Cu–Sn mineralization age, discovering that they were largely synchronous. They also found evidence that the ore-forming fluid derived from the granitic magma and that the fluid interaction with the Triassic basalt caused the Cu ore to form in the basalt.

A possible genetic model for the Kafang stratiform Cu deposit is hereby proposed: The Gejiu basalts were erupted 244.4 Ma as a post-magmatism event of the Emeishan plume, with no mineralization occurring synchronously with the eruption. Thereafter, during 85.5–83.3 Ma, the granite had intruded into the KF and LC basalts and the Gejiu Formation. The granite had evolved a K-rich hydrothermal fluid. This K-rich fluid first interacted with the dolomite, gaining Mg, and then interacted with the basalt, leaching Cu and S from the basalt and changing the minerals and the compositions (increasing K_2O and MgO contents) of the basalts. As this fluid cooled, the chalcopyrite and pyrrhotite precipitated, and the stratiform Cu ore formed within the altered basalt at 84.2–79.6 Ma.

7. Conclusions

The important conclusions from this study are as follows:

1. The eruption age of the Gejiu basalts is 244.4 Ma. However, the hydrothermal alteration (85.5–81.9 Ma) and the Cu mineralization (84.2–79.6 Ma) of the basalts are temporally related to the Cretaceous granite (85.5–83.3 Ma).
2. Based on Pb and S isotopic composition studies, the Gejiu basalts provide ore-forming materials to the Kafang stratiform Cu deposit.
3. The high amounts of K and Mg in the Gejiu basalts can be attributed to hydrothermal alteration, with the granite being the source of K and the wall-rock dolomite being the source of Mg.
4. The Gejiu basalts differ from the basalts that host typical VMS deposits, and the Kafang stratiform Cu deposit was formed by Cretaceous granite-related hydrothermal processes.

Supplementary data to this article can be found online at http://dx.doi.org/10.1016/j.oregeorev.2015.03.011.

Acknowledgments

This study was financially supported by the Crisis Mines Continued Resources Exploration Project, China Geological Survey (No. 2008186); the Guizhou 1:50000 Geological Survey Projects of Dushan, Hezhai, Jialiang and Zhouqin, Guizhou Province, China Geological Survey (No. 12120114072801); and the Guizhou 1:50000 Geological Survey Projects of Fanjingshan, Dewang, Jiangkou and Kaide, China Geological Survey (No. 1212011120622). We appreciate the assistance of Jing Hu, Guangping Bao, and Yan Huang in the trace element analyses. We thank Liang Qi, Lin Ye and Hong Zhong for their advice. We are grateful to Yulong Yang, Hongpeng Fan Pingping Liu and Chengbiao Leng for their revisions of the manuscript. Editor Franco Pirajno and two anonymous reviewers are especially thanked for their valuable comments and suggestions.

References

308 Geological Party, 1984. Geology of Tin Deposit in Gejiu Area. Metallurgical Industry Publishing House, Beijing, pp. 50–90 (in Chinese with English abstract).
Barrie, C.T., Hannington, M.D., 1999. Classification of volcanic-associated massive sulfide deposits based on host-rock composition. Rev. Econ. Geol. 8, 1–11.
Belshawet, N.S., Freedman, P.A., O'Nions, R.K., Frank, M., Guo, Y., 1998. A new variable dispersion double-focusing plasma mass spectrometer with performance illustrated for Pb isotopes. Int. J. Mass Spectrom. 181, 51–58.
Cheng, Y.B., 2012. Spatial–temporal evolution of the magmatism and mineralization in the Gejiu supergiant Sn polymetallic district and insights into several key problems. The Dissertation of China University of Geosciences, China (in Chinese with English abstract).
Cheng, Y.B., Mao, J.W., 2010. Age and geochemistry of granites in Gejiu area, Yunnan Province, SW China: constraints on their petrogenesis and tectonic setting. Lithos 120, 258–276.
Cheng, Y.B., Mao, J.W., Rusk, B., Yang, Z.X., 2012. Geology and genesis of Kafang Cu–Sn deposit, Gejiu district, SW China. Ore Geol. Rev. 48, 180–196.
Cheng, Y.B., Mao, J.W., Chang, Z.S., Pirajno, F., 2013. The origin of the world class tin-polymetallic deposits in the Gejiu district, SW China: constraints from metal zoning characteristics and ^{40}Ar–^{39}Ar geochronology. Ore Geol. Rev. 53, 50–62.
Condie, K.C., 2003. Incompatible element ratios in oceanic basalts and komatiites, tracking deep mantle sources and continental growth rates with time. Geochem. Geophys. Geosyst. 4, 1005. http://dx.doi.org/10.1029/2002GC000333.
Fang, W.X., Jia, R.X., 2011. Characteristics of the alkaline picritic volcanic rocks in the Gejiu supergiant tin–Cu deposit and their continental dynamic implications. Geotecton. Metallog. 35, 137–148 (in Chinese with English abstract).
Franklin, J.M., Sangster, D.M., Lydon, J.W., 1981. Volcanic-associated massive sulfide deposits. Economic Geology 75th Anniversary Volume, pp. 485–627.
Franklin, J.M., Gibson, H.L., Jonnason, I.R., Gallay, A.J., 2005. Volcanogenic massive sulfide deposits. Economic Geology 100th Anniversary Volume, pp. 523–560.
Hart, S.R., 1969. Rb, Cs contents and K/Rb, K/Cs ratios of fresh and altered submarine basalts. Earth Planet. Sci. Lett. 6, 295–303.
Hart, T., Gibson, H.L., Lesher, C.M., 2004. Trace element geochemistry and petrogenesis of felsic volcanic rocks associated with volcanogenic Cu–Zn–Pb massive sulfide deposits. Econ. Geol. 99, 1003–1013.
Hofmann, A.W., Jochum, K.P., Seufert, M., White, W.M., 1986. Nb and Pb in oceanic basalts: new constraints on mantle evolution. Earth Planet. Sci. Lett. 79, 33–45.
Large, R.R., McPhie, J., Gemmell, J.B., Herrmann, W., Davidson, G.J., 2001. The spectrum of ore deposit types, volcanic environments, alteration halos, and related exploration vectors in submarine volcanic successions: some examples from Australia. Econ. Geol. 96, 1037–1054.
Le Bas, M.J., 2000. IUGS reclassification of the high-Mg and picritic volcanic rocks. J. Petrol. 40, 1467–1470.
Li, Z.R., 1991. Geological characteristics of the Kafang Cu deposit in the basalt, Gejiu, Yunnan Province. Geochimica 2, 170–177 (in Chinese with English abstract).
Li, Y.S., Qin, D.X., Dang, Y.T., Xue, C.D., Tan, S.C., Hong, T., 2006. Mineralizations in basalts of the Gejiu tin deposit in Yunnan Province. J. Jilin Univ. (Earth Sci. Ed.) 36, 326–335 (in Chinese with English abstract).
Li, Z.X., Wartho, J.A., Occhipinti, S., Zhang, C.L., Li, X.H., Wang, J., Bao, C.M., 2007. Early history of the eastern Sibao orogen (South China) during the assembly of Rodinia: new $^{40}Ar/^{39}Ar$ dating and U–Pb SHRIMP detrital zircon provenance constraints. Precambrian Res. 159, 74–94.
Li, Y.S., Qin, D.X., Zou, T., Jia, F.J., Wan, C.Y., 2008. Geochemical features and tectonic setting of the Ladinian basalt in Gejiu, Yunnan Province. J. Jilin Univ. (Earth Sci. Ed.) 4, 624–630 (in Chinese with English abstract).
Li, X.H., Liu, Y., Li, Q.L., Guo, C.H., Chamberlain, K.R., 2009a. Precise determination of Phanerozoic zircon Pb/Pb age by multicollector SIMS without external standardization. Geochem. Geophys. Geosyst. 10, Q04010. http://dx.doi.org/10.1029/2009GC002400.
Li, Y.S., Qin, D.X., Guo, N.N., Luo, X., Zhou, T., Wan, C.Y., Zhou, N.S., 2009b. Geotectonic setting and mineralization significance of Indo-Chinese epoch basalts in eastern Gejiu of Yunnan. Nonferrous Met. 61, 104–109 (in Chinese with English abstract).
Liang, Q., Jing, H., Gregoire, D.C., 2000. Determination of trace elements in granites by inductively coupled plasma mass spectrometry. Talanta 51, 507–513.
Lu, H.J., 2008. An approach to geologic features and genesis of basic volcanic rock-type Cu deposit in eastern Gejiu zone. Nonferrous Met. 60, 22–33 (in Chinese with English abstract).
Ludwig, K.R., 2003. ISOPLOT 3.0: a geochronological toolkit for Microsoft Excel. Berkeley Geochronol. Cent. Spec. Publ. 4, 71.
Mao, J.W., Cheng, Y.B., Guo, C.L., Yang, Z.X., Zhao, H.J., 2008. Gejiu tin polymetallic ore-field: deposit model and discussion. Acta Geol. Sin. 81, 1456–1468 (in Chinese with English abstract).
Meschede, M., 1986. A method of discrimination between different types of mid-ocean ridge basalts and continental tholeiites with the Nb–Zr–Y diagram. Chem. Geol. 56, 207–218.
Metcalfe, I., 2006. Palaeozoic and Mesozoic tectonic evolution and palaeogeography of East Asian crustal fragments: the Korean Peninsula in context. Gondwana Res. 9, 24–46.
Ohmoto, H., 1972. Systematics of sulfur and carbon isotopes in hydrothermal ore deposits. Econ. Geol. 67, 551–579.
Ohmoto, H., 1986. Stable isotope geochemistry of ore deposits. Rev. Mineral. Geochem. 16, 491–559.
Páez, G.N., Ruiz, R., Guido, D.M., Jovic, S.M., Schalamuk, I.B., 2010. The effects of K-metasomatism in the Bahía Laura volcanic complex, Deseado massif. Chem. Geol. 273, 300–313.
Pearce, J.A., 1996. A user's guide to basalt discrimination diagrams. In: Wyman, D.A. (Ed.), Trace Element Geochemistry of Volcanic Rocks, Applications for Massive Sulphide Exploration. Geological Association of Canada, Short Course Notes 12, pp. 79–113.
Pearce, J.A., Cann, J.R., 1973. Tectonic setting of basic volcanic rocks determined using trace element analyses. Earth Planet. Sci. Lett. 19, 290–300.
Qian, Z.k., 2012. Mineralization, geochronology and genesis of the interbedded oxide orebodies in the Gejiu super-large tin–copper polymetallic deposit. The Dissertation

of Graduate University of Chinese Academy of Sciences, China (in Chinese with English abstract).
Qin, D.X., Li, Y.S., 2008. Studies on the Geology of the Gejiu Sn–Cu Deposit. Science Press, Beijing, pp. 1–180 (in Chinese with English abstract).
Rollinson, H., 1993. Using Geochemical data: Evaluation, Presentation, Interpretation. Longman, Singapore.
Shellnutt, J.G., Jahn, B.M., 2011. Origin of late Permian Emeishan basaltic rocks from the Panxi region (SW China): implications for the Ti-classification and spatial–compositional distribution of the Emeishan flood basalts. J. Volcanol. Geotherm. Res. 199, 85–95.
Shellnutt, J.G., Denyszyn, S.W., Mundil, R., 2012. Precise age determination of mafic and felsic intrusive rocks from the Permian Emeishan large igneous province (SW China). Gondwana Res. 22, 118–126.
Staudigel, H., Hart, S.R., 1983. Alteration of basaltic glass: mechanisms and significance for the oceanic crust–seawater budget. Geochim. Cosmochim. Acta 47, 337–350.
Sun, S.S., McDonough, W.F., 1989. Chemical and isotopic systematics of oceanic basalts: implications for mantle composition and processes. Geol. Soc. Lond., Spec. Publ. 42, 313–345.
Swinden, H.S., 1991. Paleotectonic settings of volcanogenic massive sulphide deposits in the Dunnage zone, Newfoundland Appalachians. Can. Inst. Min. Metall. Bull. 84, 59–69.
Tan, S.C., Qin, D.X., Zhao, X.Q., Li, J., Xia, J.S., Jiang, S.D., Cui, Y.L., Zhang, X.S., 2006. Submarine basic volcano-sedimentary Sn–Cu–Zn(Au) deposit metallogenic series of the Middle-Later Indo-Chinese epoch in Gejiu tin deposit. Geol. Prospect. 1, 43–50 (in Chinese with English abstract).
Wang, X.K., 1993. Geologic and geochemical characteristics of Gejiu Kafang volcanic rock. J. Kunming Inst. Technol. 18, 1–9 (in Chinese with English abstract).
Wang, C.Y., Zhou, M.F., Qi, L., 2007. Permian flood basalts and mafic intrusions in the Jinping (SW China)–Song Da (northern Vietnam) district: mantle sources, crustal contamination and sulfide segregation. Chem. Geol. 243, 317–343.
Winchester, J.A., Floyd, P.A., 1977. Geochemical discrimination of different magma series and their differentiation products using immobile elements. Chem. Geol. 20, 325–343.
Wood, D.A., 1980. The application of a Th–Hf–Ta diagram to problems of tectonomagmatic classification and to establishing the nature of crustal contamination of basaltic lavas of the British tertiary volcanic province. Earth Planet Sci. Lett. 50, 11–30.
Wyman, D.A., 2000. High-precision exploration geochemistry: applications for volcanogenic massive sulfide deposits. Aust. J. Earth Sci. 47, 861–871.
Xu, Y.G., He, B., Chung, S.L., Menzies, M.A., Frey, F.A., 2004. Geologic, geochemical, and geophysical consequences of plume involvement in the Emeishan flood-basalt province. Geology 32, 917.
Xue, C.D., 2002. The space–time structure model of the Gejiu super large Tin–Cu–polymetallic deposit. The Dissertation of Kunming University of Science and Technology, China (in Chinese with English abstract).
Yang, Z.X., Mao, J.W., Chen, M.H., Cheng, Y.B., Chang, Y., 2010. Geology, geochemistry and genesis of Kafang copper deposit in Gejiu, Yunnan Province. Acta Petrol. Sin. 26, 830–844 (in Chinese with English abstract).
YBGMR (Yunnan Bureau of Geology and Mineral Resources), 1982. Regional Geology of Yunnan Province. Geological Publishing House, Beijing (in Chinese with English abstract).
Zhang, H.F., Sun, M., Zhou, X.H., Fan, W.M., Zhai, M.G., Yin, J.F., 2002. Mesozoic lithosphere destruction beneath the North China craton: evidence from major-, trace-element and Sr–Nd–Pb isotope studies of Fangcheng basalts. Contrib. Mineral. Petrol. 144, 241–253.
Zhang, H., Tong, X., Wu, J.D., Luo, T.Y., Tao, Y., Zhu, D., 2007. Gejiu tin-polymetallic ore deposit: an example of landing of Red Sea-type submarine hydrothermal deposition. Acta Mineral. Sin. 27, 335–341 (in Chinese with English abstract).
Zhang, H., Fang, W.X., Zhang, G.S., Gan, F.W., Wei, N., Guo, Y.Q., 2009. Facies sequence re-establishment and metallogenic analyses of Middle Triassic meta-volcanic rocks in the Kafang ore district, Gejiu, Yunnan. Geol. China 36, 1322–1330 (in Chinese with English abstract).
Zhang, J., Mao, J.W., Cheng, Y.B., Li, X.L., 2012a. ^{40}Ar–^{39}Ar isotopic age study of phlogopite from Kafang altered basalt in Gejiu of Yunnan Province and its significance. Geol. China 39, 1648–1656 (in Chinese with English abstract).
Zhang, J., Mao, J.W., Cheng, Y.B., Li, X.L., 2012b. ^{40}Ar–^{39}Ar phlogopite dating of stratified ore body and muscovite dating of greisens from Xinshan granite intrusion of Kafang tin–copper deposit in Gejiu area, Yunnan Province. Mineral Deposits 39, 1149–1162 (in Chinese with English abstract).
Zhang, J.W., Huang, Z.L., Luo, T.Y., Qian, Z.K., Zhang, Y., 2013. Origin of early Triassic rift-related alkaline basalts from Southwest China: age, isotope, and trace-element constraints. Int. Geol. Rev. 55, 1162–1178.
Zhang, J.W., Huang, Z.L., Luo, T.Y., Yan, Z.F., 2014. LA-ICP-MS zircon geochronology and platinum-group elements characteristics of the Triassic basalts, SW China: implications for post-Emeishan large igneous province magmatism. J. Asian Earth Sci. 87, 69–78.
Zhuang, Y.Q., Wang, R.Z., Yang, S.P., Yin, J.M., 1996. Tin–Copper Polymetallic Deposits. Earthquake Publishing House, Beijing (in Chinese).